A New Class of Single-Material, Non-Reciprocal Microactuators

Charlie Maslen, Azarmidokht Gholamipour-Shirazi,* Matthew D. Butler, Jindrich Kropacek, Ivan Rehor, and Thomas Montenegro-Johnson

A crucial component in designing soft actuating structures with controllable shape changes is programming internal, mismatching stresses. In this work, a new paradigm for achieving *anisotropic dynamics* between isotropic end-states—yielding a non-reciprocal shrinking/swelling response over a full actuation cycle—in a microscale actuator made of a single material, purely through microscale design is demonstrated. Anisotropic dynamics is achieved by incorporating micro-sized pores into certain segments of the structures; by arranging porous and non-porous segments (specifically, struts) into a 2D hexagonally-shaped microscopic poly(*N*-isopropyl acrylamide) hydrogel particle, the rate of isotropic shrinking/swelling in the structure is locally modulated, generating global anisotropic, non-reciprocal, dynamics. A simple mathematical model is introduced that reveals the physics that underlies these dynamics. This design has the potential to be used as a foundational tool for inducing non-reciprocal actuation cycles with a single material structure, and enables new possibilities in producing customized soft actuators and modular anisotropic metamaterials for a range of real-world applications, such as artificial cilia.

C. Maslen, J. Kropacek, I. Rehor
Department of Chemical Engineering
University of Chemistry and Technology
Prague 166 28, Czech Republic
A. Gholamipour-Shirazi, M. D. Butler, T. Montenegro-Johnson
School of Mathematics
College of Engineering and Physical Sciences
University of Birmingham
Birmingham B15 2TT, UK
E-mail: a.g.shirazi@bham.ac.uk
I. Rehor
Institute of Organic Chemistry and Biochemistry of the Czech Academy of Sciences
Flemingovo nam. 2, Prague 160 00, Czech Republic

1. Introduction

Miniaturization of actuators to sub-millimeter scales requires new construction approaches. This is because traditional principles, based on rigid parts connected by joints and hinges, both lose efficacy at small scales—owing to the dominance of surface (adhesive) forces—and also are subject to the inherent scale limit at which individual components can be produced and integrated.[1] Replacing joints with flexible parts that actuate via deformation is a widely adopted approach to small-scale actuation, as exemplified in the MEMS industry.[2]

Recently, a new class of micro-actuators was introduced,[3] relying on soft materials (such as elastomers and hydrogels), capable of active change of their shape and/or volume when exposed to appropriate stimuli. The simplicity of these micro-actuators' fabrication, variety of actuation-inducing stimuli, and their soft, compliant, biocompatible nature holds promise for their utilization in many applications. One particular field of interest is in medicine, with potential uses such as minimally invasive surgery, telemetry, and targeted delivery.[4]
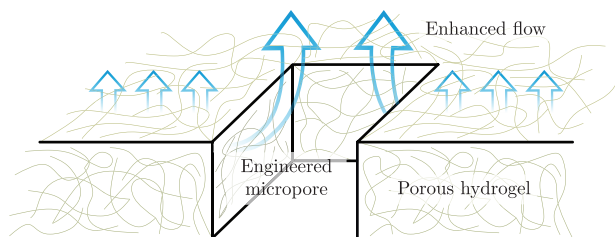
Thermo-responsive hydrogels represent promising materials for the construction of micro-actuators because they provide a well-controlled volumetric response with a high amplitude.[5,6] Temperature-dependent poly(*N*-isopropyl acrylamide) (pNIPAM) hydrogels and its derivatives have been used to fabricate a variety of smart sensors and actuators (among them[4,7,8]). Loading the pNIPAM hydrogel with a species of high specific absorption—such as graphitic material, dyes, or plasmonic nanoparticles—enables remote heating of the gel by illumination with a high-intensity light source.[9,10]

The swelling and shrinking of homogeneous stimuli-responsive hydrogels typically involves an isotropic change of volume. However, this behavior greatly limits the scope of applications.[4] Hydrogel actuators are typically required to exhibit complex shape changes, such as bending,[11–13] buckling,[14,15] and folding.[16–18] Hence, numerous efforts were reported, to overcome this limitation, and used various strategies to create mismatched stresses within the hydrogel network (e.g., soft vs stiff, swelling vs non-swelling).[6,19–21]

**ADVANCED
SCIENCE NEWS**

www.advancedsciencenews.com

{M} acro-
molecular

Rapid Communications

www.mrc-journal.de

Figure 1. Schematic showing a heterogeneous nanoporous hydrogel, with an engineered microscale pore providing additional paths for fluid to escape/enter, resulting in an anisotropic, non-reciprocal, and global response.

However, inducing spatial anisotropy is merely a first step toward the practical application of soft micro-actuators. Controllable asymmetric actuation *in time* is of upmost importance. Micro-actuators in fluidic environments operate in the low Reynolds regime and, hence, cannot achieve net displacement of themselves, or of surrounding fluids, via time-reversible kinematics, that is, reciprocal actuation.[22] Therefore, a non-reciprocal actuation cycle is a necessary prerequisite for a micro-actuator application as a micro-pump, -mixer, -robot, or -manipulator.[23,24] Non-reciprocal actuation can be achieved by incorporating more than one degree of freedom into the micro-actuator, which imposes extra requirements on the fabrication process as well as on the control.[25,26] Alternatively, to reduce these requirements, approaches should be found where the actuation pathway during an on–off cycle of a single stimulus proceeds in a non-reciprocal manner.

Despite examples of the latter,[27–29] no general method to engineer such non-reciprocal actuation pathways currently exists. There is a lack of processes that enable the design of non-reciprocally actuating micro-systems with tailorable actuation pathways. The design principles must allow subsequent low-cost scalable fabrication of the micro-components.

Here, we introduce a generic method to create hydrogel micro-actuators with anisotropic dynamics, by precisely engineering microscopic pores to defined segments of their structures. Out-of-equilibrium isotropic volumetric changes are transferred, through this localized microscale design, to "dynamic anisotropy" (i.e., spontaneously emerging and disappearing over the course of the volumetric change) of the lithographic microobjects. This dynamic anisotropy is a generic pathway that allows these micro-actuators to realize non-reciprocal actuation.

The hydrogel actuators undergo photo-thermally–induced isotropic shrinkage and re-expansion cycles, where the solvent is being cyclically expelled from, and reabsorbed into, the gel. Upon fast heating and cooling, the solvent transfer from and into the gel is the rate limiting element of the actuation. The microstructure pores in the gel strut design accelerate the solvent transfer from and into the gel as fluid drains and, ultimately, accelerate the actuation of the porous struts compared to the non-porous ones (**Figure 1**).

This concept is inspired by previous work on homogeneous hydrogels containing microscale pores, which act to increase the rate of volumetric change.[30–32] Here we now engineer the additional micro-porous structure, locally and precisely, in order to achieve complex dynamic anisotropy and non-reciprocal actua-

tion cycles; appropriate combination of porous and non-porous segments in one structure provides non-reciprocally actuating microstructures. Notably, the entire micro-actuator is fabricated in a single step, high-throughput process and has a uniform material composition. The modular, tuneable nature of our components raises interesting possibilities for their targeted self-assembly into responsive metamaterials.

2. Results and Discussion

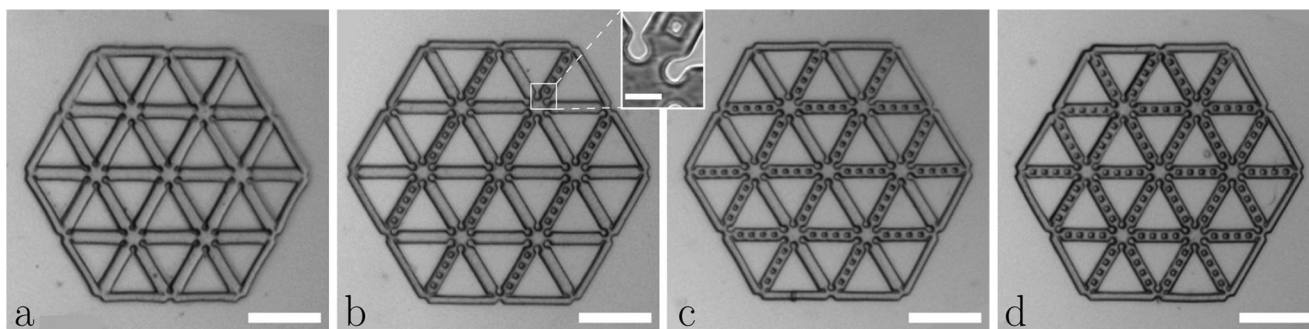### 2.1. Micro-Actuator Design and Fabrication

We present anisotropic actuation of periodically shrinking and expanding hydrogel micro-platelets (430 μm vertex to vertex distance, 30 μm height) fabricated by stop-flow lithography: a high-throughput and easy to perform continuous lithographic process.[33,34] The platelet consists of hexagonally arranged "struts" separated by triangular holes. Anisotropic responses have previously been demonstrated in macroscale hexagonal arrangements of struts.[35] **Figure 2** shows an overview of all the designs used in this study.

Each individual strut is 68 μm long and 16 μm wide and is oriented in one of three directions within the hexagonal structure. To enable greater flexibility at the joints connecting the struts through in-plane deformations, we include a thinner, 5 μm wide section at the end of each strut which connects to a hexagonal node (Figure 2 inset). Certain struts in some designs contain square pores (8.5 μm × 8.5 μm) which are arranged linearly within the struts (separated by 8.5 μm intervals). We produced four distinct designs with differing arrangements of pores within the body of the platelet (Figure 2 shows the four designs). Two arrangements are symmetrical, with either no struts containing pores, or all struts containing pores. The two other arrangements are asymmetrical. One has pores in all the struts oriented in one direction, with the other two orientations of struts being non-porous. The second arrangement has pores in the struts oriented in two out of the three directions, with the remaining struts being non-porous. Henceforth we refer to these distinct designs as: solid (all struts non-porous), porous (all struts porous), unidirectional (porous struts in one direction), and bidirectional (porous struts in two directions).

2.2. Actuation Principle and Bulk Heating

The platelets are composed of thermally-responsive pNIPAM which, when subjected to heating above its lower critical solution temperature (LCST) (≈35 °C[36]), undergoes a transition from a hydrophilic to a hydrophobic state. The result of this transition is the expulsion of water from the polymer network and accompanying macroscopic shrinkage of the platelet. When cooled below 35 °C, the hydrogel transitions to a hydrophilic state and the platelet re-swells back to its original volume as water is reabsorbed into the network.

Rapid heating of the pNIPAM is achieved by entrapping gold nanospheres (15 nm diameter) within the hydrogel network to allow photothermal heating by laser illumination (532 nm green laser light).[9,33] With a 100 W/cm² intensity of light, the platelet

ADVANCED
SCIENCE NEWS
www.advancedsciencenews.com

{M}acro-molecular
Rapid Communications
www.mrc-journal.de

Figure 2. The hexagonal particles a) solid, b) unidirectional, c) bidirectional, and d) porous. The scale bar is 100 μm. The inset shows detail of a joint and a pore, with a scale bar of 15 μm.
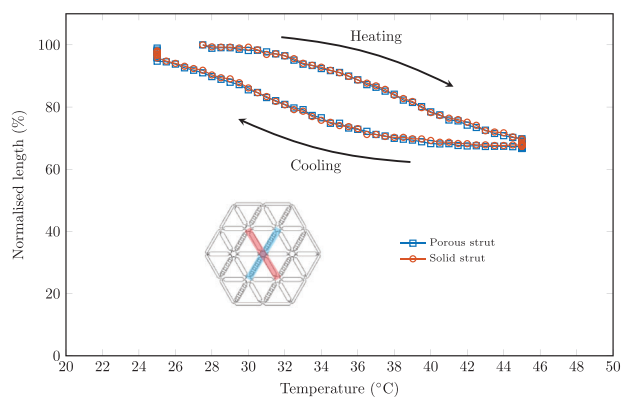
Figure 3. Shrinking and swelling of porous struts (blue) and solid struts (red) over time for the unidirectional design during equilibrium heating and cooling. The length of a strut is normalized so that it is a percentage of its initial length.

collapses rapidly (0.3 s) to 65% of its initial linear dimensions. Subsequent removal of the illumination enables rapid cooling of the platelet by dissipation of the heat to the surroundings with the gel returning to 95% of its original linear size within 1.5 s.

The length of two, non-parallel vertex–vertex distances of the central hexagon (the highlighted struts in **Figure 3**) were selected as the geometric parameters to characterize the volumetric and shape change of the platelets (the outer sections of the platelet would occasionally bend out-of-plane, therefore we omitted them from the analysis). The length of these struts was measured over time during actuation.

We first investigated the equilibrium strut lengths versus temperature dependency by changing the temperature slowly. For this, the particles were subjected to macroscopic (bulk) heating and cooling at a rate of 3 °C min⁻¹. In Figure 3, we show the results for porous and solid struts in the unidirectional design. During heating of the aqueous environment, all of the platelets collapse isotropically, which is reflected by their uniform shrinkage. Upon subsequent cooling, the gel undergoes isotropic re-swelling to its original dimensions. A hysteresis is observed in the volume versus temperature profile between heating and cooling cycles (originating from events on the molecular level inside the gel[37–39]). However, there is negligible difference between the size of porous and non-porous struts at any temperature. At this
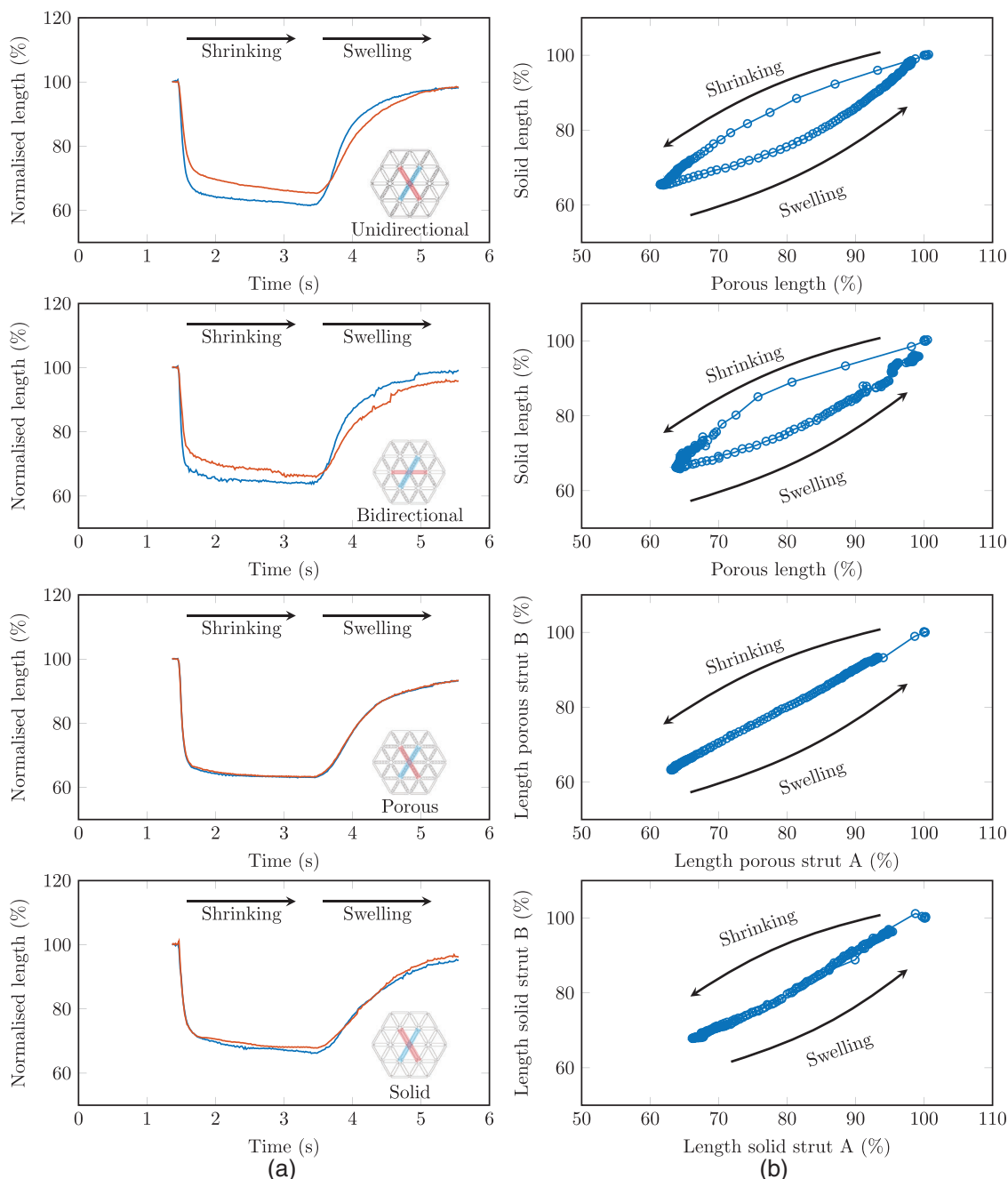
slow heating/cooling rate, the gel remains close to its equilibrium volume at any particular temperature.

2.3. Photothermal Actuation

The situation changes when the gel is instead heated and cooled rapidly by pulsed irradiation (2 s) with the 532 nm laser. The porous struts collapse significantly faster than the solid struts. Under identical illumination conditions the full collapse of the entirely solid and entirely porous platelet takes ≈0.3 s and ≈0.2 s, respectively. In this case, the collapse/swelling proceeds out-of-equilibrium: the temperature rises rapidly resulting in the expulsion of water from the gel, accompanied by corresponding conformational changes in the gel structure, with the former being the rate determining factor of the collapse/swelling process.[40] The water diffusion rate out from the collapsing, and into the swelling gel, respectively, is in part determined by the local geometry and size of the gel: larger gels respond slower to the sudden temperature changes,[41,42] since the free water diffusion from/to the central part is hindered by the surrounding gel. This is well documented by the "skin" formation effect observed with rapidly collapsing pNIPAM gels, where the surface gel layer shrinks to form a barrier, inhibiting the water escape from the gel center.[43,44] Hence, simple changes of the gel geometry, by means of its surface-to-volume ratio, would affect the out-of-equilibrium collapse and swelling rates. Therefore, the porous struts display faster collapsing and re-swelling, as the pores reduce the distance water molecules must travel from within the gel to the external environment and vice versa.

With asymmetric platelets, the shrinking is faster in the porous directions than the solid (**Figure 4**a). After removal of the laser and subsequent rapid cooling, the rate of re-swelling is similarly increased for the porous platelets and in the porous directions of asymmetric platelets compared to their solid counterparts (Figure 4a). Thus, by simple introduction of pores within the struts, the out-of-equilibrium shrinkage and swelling rate can be selectively enhanced. Therefore, the swelling and shrinking occur non-reciprocally in the asymmetric platelets, as shown by the strut length paths shown in Figure 4b, but this is not observed in the symmetric designs.

The result of these effects mean that the shape of an asymmetrically-designed platelet is distorted compared to a

ADVANCED
SCIENCE NEWS
www.advancedsciencenews.com

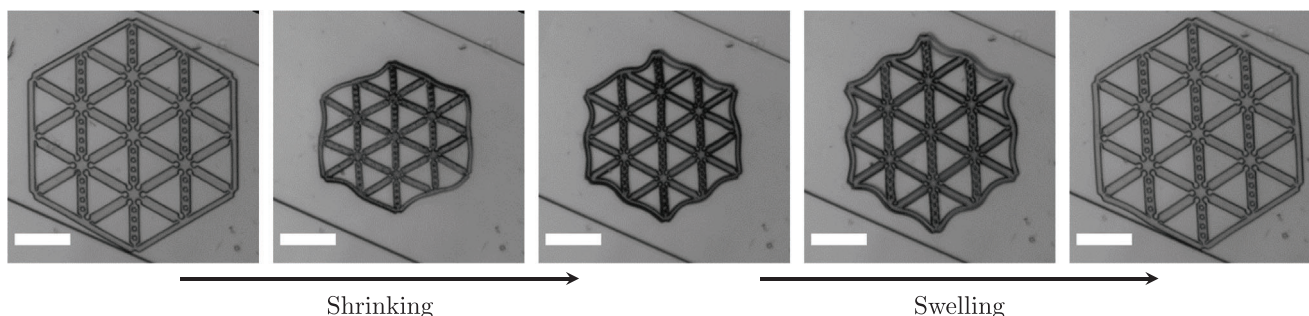acro-
olecular
Rapid Communications
www.mrc-journal.de

Figure 4. Shrinking and swelling of porous and solid struts in the different designs. The colors of the curve correspond to the highlighted struts shown in the inset; for the anisotropic designs (unidirectional, bidirectional) the porous struts are blue and the solid struts are red. The normalized strut lengths are shown a) over time and b) relative to each other. The area between two curves shows the non-reciprocity. The length of the struts were measured using the image analysis (average of seven videos-for unidirectional, two videos for bidirectional, eight videos for porous, and three video-analysis for solid) and normalized using the initial length of each strut at the beginning of the video.

perfect hexagon during shrinkage, being shorter in the porous strut directions, while upon complete collapse, the hexagonal symmetry is re-established. When the laser is turned off, the platelet expands; during this expansion, the porous struts exceed the length of the solid struts, resulting in distortion of the platelet during re-swelling as it becomes elongated in the direction of the porous struts. Eventually, after a period of slow expansion of

the platelet in which equilibrium is re-established, the hexagonal symmetry of the gel is restored. This distortion over a cycle of heating and cooling is illustrated in **Figure 5**. Occasionally certain symmetry distortions remain in the fully shrunken state, as is visible in Figure 4a for the unidirectional hexagon. We ascribe it to a slow relaxation of the structure into equilibrium, mainly overcoming the friction and viscous resistance,[45] since

**ADVANCED
SCIENCE NEWS**

www.advancedsciencenews.com

**[M] acro-
molecular
Rapid Communications**

www.mrc-journal.de

Figure 5. Breaking/recovering hexagonal symmetry during one actuation cycle. The visible lines are the side walls of the channel. The scale bar is 100 μm.
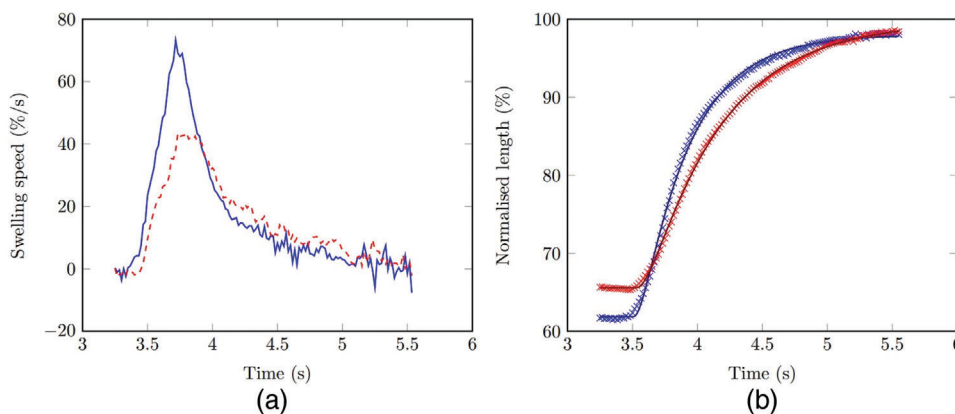
Figure 6. a) The swelling speed of the porous (blue solid curve) and solid (red dashed curve) struts of the unidirectional platelet. b) A comparison of the experimental data (crosses) with the fitting of Equation (2) (solid curves) for the porous (blue) and solid (red) struts of the unidirectional platelet.

we already proved, that the porous and non porous struts shrink identically in equilibrium (Figure 3).

Occasionally, when the laser illumination was removed and the asymmetric platelets were swelling, we observed a localized chiral instability at the connecting vertices between struts (see Supporting Information). This is likely due to struts experiencing compressive forces as they expand while being constrained due to their attachment to other slower expanding struts (or possibly encountering the walls of the channel). Compression of the struts can cause buckling, which will occur at the weakest part first: the thin regions next to the joints. The result is the formation of spiral-like twisting pattern around the struts. The symmetric platelets (fully solid or fully porous) are significantly less prone to these twists, likely due to the uniform swelling rate across the particle and symmetrical distribution of stress. We aimed to suppress this twisting, which hinders the anisotropic deformation we desire, by optimizing the composition of the gel. This was achieved by fine-tuning the amount of crosslinker in the gel pre-cursor and, hence, the stiffness of the resulting gel. Densely crosslinked gels did not exhibit twisting, but their volumetric response to heating was damped and so was the difference between the collapse/expansion rate of the solid and porous struts, reducing the anisotropic and non-reciprocal behavior of the actuation. The composition we employ thus represents a compromise, reducing the twisting instability as much as possible whilst maintaining the desired response.

2.4. Quantifying the Swelling Behavior

The swelling and shrinking dynamics seen in Figure 4a,b suggests that there is a difference between the evolution of the two types of struts after a temperature change. To quantify this difference, we first consider the speed at which the struts' lengths change. We focus on the swelling dynamics (the right-hand-side of Figure 4a) because the dynamics there can be resolved more clearly, since the evolution occurs more slowly.

Figure 6a shows an example for the calculated swelling speed of porous and solid struts in the unidirectional design. The length data plotted in Figure 4a were first smoothed to remove noise before the derivative was calculated. A clear difference between the two struts appears to be the peak swelling speed, and so we calculated this for each of the measured struts. The maximum swelling speed of each strut is presented in **Table 1**.

For the symmetric platelets, the maximum speed is equivalent in each strut, as expected; however, in the asymmetric platelets, the maximum swelling speed is noticeably higher for the porous strut than that of the solid strut (with normalized speeds 73 vs 44 % s^{-1} for unidirectional, and 68 vs 43 % s^{-1} for bidirectional). This suggests that there is a significant difference in the dynamics between the porous and solid struts.

Notably, the maximum rate of expansion is greater for all struts in asymmetric designs than symmetric designs, and this is especially pronounced for the porous struts.

Table 1. Maximum swelling speed [% s^{-1}].

Unidirectional		Bidirectional		Porous		Solid	
Porous strut	Solid strut	Porous strut	Solid strut	Porous strut	Porous strut	Solid strut	Solid strut
73.25	43.64	68.29	43.42	37.99	37.21	33.02	33.22

Table 2. The fitting parameters.

Parameter	Unidirectional		Bidirectional		Porous	Solid
	Porous strut	Solid strut	Porous strut	Solid strut	Porous strut	Solid strut
r	15.58	10.69	24.04	17.18	6.39	3.05
s	2.62	1.72	2.16	1.53	2.04	1.70
t_0	3.51	3.53	3.50	3.53	3.53	3.48
L_0	61.88	65.59	64.23	66.36	63.45	67.23
L_∞	98.02	99.72	99.08	97.94	93.59	98.07

To understand the dynamic behavior of these swelling and shrinking struts in more detail, we propose a simple mathematical model that includes the basic physics of the system. We suppose that the dominant mechanical balance governing the length change is between a spring-like elastic force, that pulls or pushes each strut toward its final length, and a viscous resistance to motion from the surrounding fluid, so that the strut length, $L(t)$, obeys an equation of the form

$$k(L - l(t)) = -\zeta \frac{dL}{dt} \tag{1}$$

where k is a material spring stiffness and ζ is a resistance that could have contributions from viscosity and friction. The spring rest length, $l(t)$, is not taken as constant, but is time-dependent. This is because, after a temperature change, the hydrogel will not be stretched/compressed until it has expelled/absorbed sufficient solute.

Theoretical models of swelling and shrinking hydrogels suggest that the motion of fluid into or out of the hydrogel is diffusive in nature.[41,46,47] The simplest models of this process suggest that the thickness of a hydrogel evolves as the sum of exponentially decaying modes (see Section 4.1.1 of ref. [46]). We assume that our spring rest length behaves in a similar manner, and for simplicity only consider the first (largest) mode, so that $l(t) = A + Be^{-st}$, for some constants A and B, with s being the rate of decay toward the equilibrium length at that temperature. We expect this rate to depend on the geometry of the hydrogel structure, and may increase as the maximum distance to the nearest free surface decreases or as the fluid viscosity decreases.[41,44,46]

We therefore find that our model predicts the evolution of the length of one strut from an initial length L_0 to a final length L_∞ to be

$$L(t) = L_\infty + (L_0 - L_\infty) \frac{re^{-s(t-t_0)} - se^{-r(t-t_0)}}{r - s} \tag{2}$$

where the dynamics begin at a time $t = t_0$, $r = k/\zeta$ is the elastic rebound rate of the strut and s is the rate that determines the evolution of the natural spring length.

We fitted Equation (2) to experimental data from the reswelling of the platelets after removal of the laser (i.e., the right-hand-side of the curves in Figure 4a). The five fitting parameters were the rates r and s, the initial and final lengths L_0 and L_∞, and the start time t_0. Note that in Equation (2) there is a symmetry between the rates r and s; we choose to take $s < r$ (so that the elastic rebound occurs faster than the fluid absorption) because comparing two platelets with different stiffnesses suggest that the larger of the two rates increases with the stiffness k, and therefore corresponds to r (see Supporting Information).

The resulting fitting parameters are presented in **Table 2**, with examples of fitting curves compared to the data shown in Figure 6b (see Supporting Information, for the comparison for other designs). Note that the values determined for the actuation time, t_0, are consistent between the two struts in each platelet, and the normalized final lengths, L_∞, are all near $L = 100$, which is consistent with the platelets eventually regaining their initial size.

Looking at the swelling rates found for the asymmetric designs in Table 2, we see clear differences between the two types of strut. First, the values of the faster elastic rebound rate, r, are higher in porous struts than in solid struts; in both the unidirectional and bidirectional designs, the porous struts have a value of r that is $\approx$40–45% larger than the solid struts. Similarly, the slower fluid absorption rate, s, is larger in the porous struts for both asymmetric designs, being 52% and 41% larger in the unidirectional and bidirectional platelets, respectively. From our theoretical model description, we see that together these suggest that the porous struts can absorb fluid and swell faster than the solid struts.

The increase in the fluid absorption rate, s, in the porous struts compared to the solid ones is expected, since the porous struts have a greater surface area with which to absorb fluid and the fluid has less distance to travel within the hydrogel to cause it to swell. The increase in the elastic response rate, r, however, is perhaps less intuitive. Adding holes to a strut is likely to reduce the stiffness k of a strut, but also may reduce the resistance ζ since there is a decrease in the area of the outer surface that may experience friction drag. The rate r is the ratio of these two contributions and so it is not clear a priori whether it should

**ADVANCED
SCIENCE NEWS**

www.advancedsciencenews.com

[M]acro-
olecular
Rapid Communications

www.mrc-journal.de

increase or decrease in porous struts compared to solid struts. Our results show that its value increases, suggesting that the addition of pores leads to reduced resistance that speeds up the early-time swelling of the struts.

This increase in swelling response rates is also seen when comparing the two symmetric structures, where porous struts also respond faster than solid struts. However, when comparing the values of these rates to similar struts in the asymmetric designs, we see that the early-time fast evolution, characterized by the elastic response rate r, occurs more quickly in the asymmetric designs; the slow rate, s, does not appear to vary as significantly (if at all) between symmetric and asymmetric designs. This suggests that the asymmetry strongly affects the evolution of the length of the struts at early times after a temperature change, but has less effect on the overall timescale for swelling.

This interpretation means that the overall dynamics of the swelling is predominantly governed by the speed at which the hydrogel can expel water from its interior, since the elastic rebound rate is faster. In the porous struts, the water can escape more easily as it has less distance to travel to the edge and can escape through the manufactured pores, resulting in an increase in the rate s, and faster swelling behavior. The damped-spring behavior from the competition between elasticity and viscous or frictional resistance plays a smaller role, but is important at early times; the corresponding rate r is larger in porous struts compared to solid ones and asymmetric designs compared to symmetric. It is not entirely clear why this is, but possibilities include a reduced area for frictional stresses to act upon and modified external fluid flow due to the presence of pores and/or anisotropic deformation.

The proposed simple model for the extension and retraction of the hydrogel struts captures the strut length dynamics very well and has given key insights into the difference between the different strut and design types. We note, however, that this model does not include the full physics involved in the experimental process. For example, the model struts are treated independently from one another, when they are in fact interconnected. This effect cannot be quantified by our model, but surely affects the calculated rates and may explain the difference between symmetric and asymmetric platelet designs.

2.5. Applications as Microfluidic Manipulators

The use of site-specific arrangements of responsive polymer self-assemblies has been reported for macroscopic actions as seen in actuator functions of surface hexagonal microscopic gel arrays.[48] Here, the hexagonal design of the non-symmetrical platelets makes them applicable as micro-actuators. To understand how such an actuator will work, it is important to know how the hexagonal particle deforms during an actuation cycle. Therefore, we tracked the respective positions of various vertex pairs in the structure to understand better their respective motion. The motion tracking of three corners (B, C, and D) with respect to one corner (A), is shown in **Figure 7**. We see that the gel undergoes a non-reciprocal shape change: for example, the path of vertex B follows a loop with respect to vertex A. This non-reciprocal behavior will result in a net displacement of the surrounding fluid over a cycle, and so it is possible that the hexagonal particle could
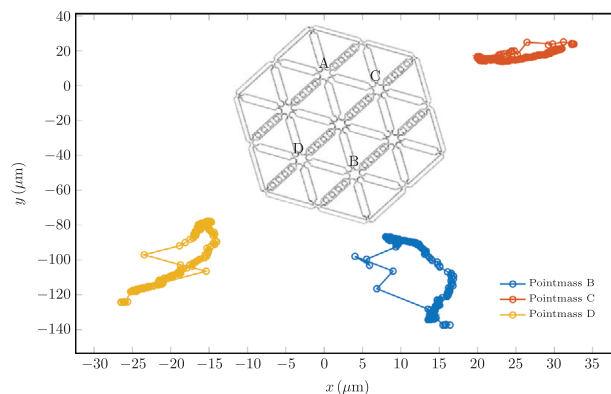
Figure 7. Motion tracking of three vertices (B, C, and D) with respect to one vertex (A), average of eight video analyses.
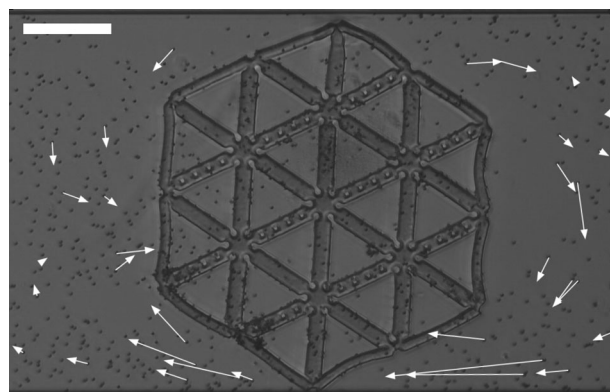
Figure 8. Displacements of tracer particles after eight actuation cycles of the platelet (1 s pulse and 4 s recovery). Scale bar is 100 μm.

be used for mixing or pumping the fluid in the channel. We turn to investigate this possibility now.

To track the surrounding fluid behavior, the channel was filled with microspheres and the hexagonal particle was kept in place by having one of its vertices attached to the channel wall (see Experimental Section). Following the procedure of Section 2.2, the platelet undergoes cyclic actuation cycles by pulsed irradiation of the platelet with laser light, and transport of the microspheres is observed (**Figure 8**). Notably, the performance of the platelet as a pump is poor, however, some degree of mixing is clearly visible. The low-cost and high-throughput method of fabrication and the material homogeneity of the platelet represents an advancement in the simplification of production of non-reciprocal micro-actuators with practical applications.

3. Conclusion

We create microscale actuators from a single responsive material which exhibit dynamic anisotropy. This is achieved via a repeatable, engineerable process of manufacturing a microscale pore structure to locally modulate the rate of isotropic swelling/shrinking of substructures within the actuator, causing out-of-equilibrium shape anisotropies. This method, in turn, provides a generic pathway for creating micro-actuators with

ADVANCED
SCIENCE NEWS

www.advancedsciencenews.com

[M] acro-
molecular
Rapid Communications

www.mrc-journal.de

non-reciprocal periodic dynamics from a single material, in a single step, purely through the geometry of the design.

In particular, we have reported on the behavior of a 2D hexagon-shaped microscopic poly(N-isopropyl acrylamide) hydrogel particle during heating and cooling cycles that cause it to shrink and re-swell. Combining two strut types, one entirely solid and the other containing manufactured microscale pores, within one hydrogel particle we observed dynamic anisotropic shape changes, leading to non-reciprocal actuation over the beat cycle. A simple mathematical model of the re-swelling process highlighted the faster rate of swelling within the porous struts compared to the solid struts, and suggested that this was because the increased surface-to-volume ratio upon the addition of pores allows fluid to more easily absorb into the hydrogel microstructure, which is the process that largely limits the dynamics. We also showed that the non-reciprocal collapse–re-swelling cycle generates a net motion in the surrounding bulk fluid in the channel, with potential to act as a microfluidic manipulator.

The modularity of our structure opens the interesting future possibility to create larger responsive structures with target properties via directed self-assembly. This might, for instance, find application in responsive metamaterials.[49,50] Indeed, although in our work we sought to suppress the chiral buckling instability observed in our structures, one can imagine engineering responsive materials to activate this instability upon stimulus, for instance changing the optical or wave guiding properties of the material. At a global scale, it may even be possible to induce these instabilities as a kind of dynamic topological defect that moves through the structure.

We are convinced that our work on this foundational, single-material element helps to create an exciting avenue for developing future soft microrobotic devices in biomedical, biomechanical, or lab-on-a-chip applications, as well as inspiring the design of new microfluidic devices that can mix, sort, and circulate fluid.

4. Experimental Section

Chemicals: N-isopropyl acrylamide (NIPAm), N, N'-methylenebisacrylamide (MBAA), lithium phenyl-2,4,6-trimethyl-benzoyl phosphinate (LAP), Poly (ethylene glycol) methyl ether thiol, Polyethylene glycol 200, Gelatin methacryloyl, 2 μm polystyrene microspheres, Tween 20, and Pluronic F127 were purchased from Sigma Aldrich and used as received. Tetrachloroaurate trihydrate ($HAuCl_4.3H_2O$) was purchased from Alfa Aesar. SYLGARD 184 silicone elastomer kit (elastomer base + curing agent), used for the fabrication of polydimethylsiloxane (PDMS) microfluidic channels, was purchased from Dow Corning. Reverse osmosis water (MilliQ) was used for all experiments (18.2 MΩ at 25 °C).

Preparation of Pre-Gel: In a vial, 8 mg of MBAA (solid powder) was weighed, and 100 μL of PEG 200 (liquid) was added. The mixture was sonicated for 5 min to dissolve the components. 48 mg of NIPAm (solid powder) was added and the mixture was again sonicated for 5 min. 30 μL of colloidal gold nanoparticles (synthesized the same day, according to ref. [33]) was added to the mixture and again sonicated for 5 min. 1.5 mg) LAP (solid powder), was weighed and added to the mixture in the last step and the mixture was again sonicated for 5 min. Before being used in the experiment, the mixture was centrifuged to remove any air bubbles and dust.

Stop-Flow Lithography: To produce hydrogel microparticles, the mixture was processed in stop-flow lithography.[34] The channel was then purged with an aqueous Pluronic solution (5 wt%) and the microparticles were collected in a PCR tube. They were washed and centrifuged several times with aqueous Pluronic solution (5 wt%) to remove the remaining pre-gel and stored in the fridge (4 °C).

Equilibrium Heating/Cooling: The inner surface of a flat glass capillary (50 × 5 × 0.5 mm) was spin-coated horizontally (2000 rpm, 1 min) with PDMS (weight ratio base: curing agent: petroleum ether 10: 1: 10). After curing, the capillary was filled with particles in Pluronic (5 wt%) dispersion and sealed with UV curable glue. The capillary containing particles was placed on a Peltier stage (LTS 120, Linkam scientific instruments Ltd., UK) for temperature control. The Peltier stage was mounted on an optical microscope (ECLIPSE Ti2, Nikon Instruments Inc., U.S.A.). The temperature of the sample was increased and decreased at the rate of 3 °C min^{-1} with an accuracy of ± 0.1 °C. Images were taken every 10 s. The images of the particles were analyzed using ImageJ (version 1.53a; National Institutes of Health, Bethesda, Maryland, USA) and Tracker (ver. 6.0.8, Open Source Physics (OSP)).

Photothermal Actuation and Analysis of Microgel: The mixture of the microparticles (dispersed in Pluronic 5 wt%) was placed inside the reservoir, Figure S4, Supporting Information, and drawn into the channel using a syringe pump (VIT-FIT, LAMBDA Instruments CZ s.r.o., Czechia) and actuated by laser, described elsewhere.[33] To fix particles within the channel, particles were dispersed in a Gelatin methacryloyl solution (10 wt% in water) containing (2 wt%) LAP. After being drawn into the channel, a vertex of the platelet was irradiated with 20 μm diameter beam of UV-light, as in stop-flow lithography. The channel was then purged with Pluronic (5 wt%) solution containing a 1000 × dilution of 2 μm polystyrene tracer particles. Images were taken of the particle deformation, using IC Capture (ver.2.5.1547.4007, The Imaging Source) and later were analyzed and tracked using ImageJ (version 1.53a; National Institutes of Health, Bethesda, Maryland, USA) and Tracker (ver. 6.0.8, Open Source Physics (OSP)) to extract the strut lengths and vertex positions.

Vertex Trajectories, Mixing: The platelet was confined in the microfluidic channel, immersed in a gelatin pre-cursor solution. By irradiation with UV light, localized to one vertex, polymerization of the pre-cursor was induced which forms a hydrogel anchor, fixing the platelet to the channel at the irradiated vertex. The channel was then washed with Pluronic solution containing polystyrene microspheres (2 μm) to remove the pre-cursor and enable visualization of any fluid motion.

Supporting Information

Supporting Information is available from the Wiley Online Library or from the author.

Conflict of Interest

The authors declare no conflict of interest.

Data Availability Statement

The data that support the findings of this study are available from the corresponding author upon reasonable request.

[1] S. Nocentini, C. Parmeggiani, D. Martella, D. S. Wiersma, *Adv. Opt. Mater.* **2018**, *6*, 1800207.

[2] L. Hines, K. Petersen, G. Z. Lum, M. Sitti, *Adv. Mater.* **2017**, *29*, 13.

[3] M. C. Koetting, J. T. Peters, S. D. Steichen, N. A. Peppas, *Mater. Sci. Eng., R* **2015**, *93*, 1.

[4] L. Ionov, *Mater. Today* **2014**, *17*, 494.

[5] J. F. Mano, *Adv. Eng. Mater.* **2008**, *10*, 515.

[6] Y. Zhang, S. Xie, D. Zhang, B. Ren, Y. Liu, L. Tang, Q. Chen, J. Yang, J. Wu, J. Tang, J. Zheng, *Eng. Sci.* **2019**, *6*, 1.

[7] H. Yuk, S. Lin, C. Ma, M. Takaffoli, N. X. Fang, X. Zhao, *Nat. Commun.* **2017**, *8*, 14230.

[8] M. E. Harmon, M. Tang, C. W. Frank, *Polymer* **2003**, *44*, 4547.

[9] S. R. Sershen, G. A. Mensing, M. Ng, N. J. Halas, D. J. Beebe, J. L. West, *Adv. Mater.* **2005**, *17*, 1366.

[10] E. Lee, H. Lee, S. I. Yoo, J. Yoon, *ACS Appl. Mater. Interfaces* **2014**, *6*, 16949.

[11] A. Nishiguchi, A. Mourran, H. Zhang, M. Möller, *Adv. Sci.* **2018**, *5*, 1700038.

[12] Q. L. Zhu, C. Du, Y. Dai, M. Daab, M. Matejdes, J. Breu, W. Hong, Q. Zheng, Z. L. Wu, *Nat. Commun.* **2020**, *11*, 5166.

[13] S. Maeda, Y. Hara, T. Sakai, R. Yoshida, S. Hashimoto, *Adv. Mater.* **2007**, *19*, 3480.

[14] J. Kim, J. A. Hanna, M. Byun, C. D. Santangelo, R. C. Hayward, *Science* **2012**, *335*, 1201.

[15] Q. L. Zhu, C. F. Dai, D. Wagner, O. Khoruzhenko, W. Hong, J. Breu, Q. Zheng, Z. L. Wu, *Adv. Sci.* **2021**, *8*, 2102353.

[16] L. Ionov, *Soft. Matter.* **2011**, *7*, 6786.

[17] J. C. Breger, C. Yoon, R. Xiao, H. R. Kwag, M. O. Wang, J. P. Fisher, T. D. Nguyen, D. H. Gracias, *ACS Appl. Mater. Interfaces* **2015**, *7*, 3398.

[18] C. N. Zhu, C. Y. Li, H. Wang, W. Hong, F. Huang, Q. Zheng, Z. L. Wu, *Adv. Mater.* **2021**, *33*, 2008057.

[19] Y. Ouyang, G. Huang, J. Cui, H. Zhu, G. Yan, Y. Mei, *Chem. Mater.* **2022**, *34*, 9307.

[20] Z. L. Wu, M. Moshe, J. Greener, H. Therien-Aubin, Z. Nie, E. Sharon, E. Kumacheva, *Nat. Commun.* **2013**, *4*, 1586.

[21] D. Jiao, Q. L. Zhu, C. Y. Li, Q. Zheng, Z. L. Wu, *Acc. Chem. Res.* **2022**, *55*, 1533.

[22] E. M. Purcell, *Am. J. Phys.* **1977**, *45*, 3.

[23] S. Palagi, P. Fischer, *Nat. Rev. Mater.* **2018**, *3*, 113.

[24] D. J. Laser, J. G. Santiago, *J. Micromech. Microeng.* **2004**, *14*, 6.

[25] Z. Zhu, E. Senses, P. Akcora, S. A. Sukhishvili, *ACS Nano* **2012**, *6*, 3152.

[26] W. Wang, J. Y. Lee, H. Rodrigue, S. H. Song, W. S. Chu, S. H. Ahn, *Bioinspiration Biomimetics* **2014**, *9*, 4.

[27] A. Mourran, H. Zhang, R. Vinokur, M. Möller, *Adv. Mater.* **2017**, *29*, 2.

[28] M. Lahikainen, H. Zeng, A. Priimagi, *Soft Matter.* **2020**, *16*, 5951.

[29] H. Zhang, L. Koens, E. Lauga, A. Mourran, M. Möller, *Small* **2019**, *15*, 46.

[30] G. Huerta-Angeles, K. Hishchak, A. Strachota, B. Strachota, M. Šlouf, L. Matějka, *Eur. Polym. J.* **2014**, *59*, 341.

[31] J. Chen, H. Park, K. Park, *J. Biomed. Mater. Res.* **1999**, *44*, 53.

[32] T. Spratte, C. Arndt, I. Wacker, M. Hauck, R. Adelung, R. R. Schröder, F. Schütt, C. Selhuber-Unkel, *Adv. Intell. Syst.* **2022**, *4*, 2100081.

[33] I. Rehor, C. Maslen, P. G. Moerman, B. G. Van Ravensteijn, R. Van Alst, J. Groenewold, H. B. Eral, W. K. Kegel, *Soft Rob.* **2021**, *8*, 10.

[34] D. Dendukuri, S. S. Gu, D. C. Pregibon, T. A. Hatton, P. S. Doyle, *Lab Chip* **2007**, *7*, 818.

[35] J. Mueller, J. A. Lewis, K. Bertoldi, *Adv. Funct. Mater.* **2022**, *32*, 2105128.

[36] H. G. Schild, *Prog. Polym. Sci.* **1992**, *17*, 163.

[37] G. Liu, G. Zhang, *J. Phys. Chem. B* **2005**, *109*, 743.

[38] H. Cheng, L. Shen, C. Wu, *Macromolecules* **2006**, *39*, 2325.

[39] Y. Lu, K. Zhou, Y. Ding, G. Zhang, C. Wu, *Phys. Chem. Chem. Phys.* **2010**, *12*, 3188.

[40] M. J. Junk, W. Li, A. D. Schlüter, G. Wegner, H. W. Spiess, A. Zhang, D. Hinderberger, *J. Am. Chem. Soc.* **2011**, *133*, 10832.

[41] T. Tanaka, D. J. Fillmore, *J. Chem. Phys.* **1979**, *70*, 1214.

[42] T. Tanaka, E. Sato, Y. Hirokawa, S. Hirotsu, J. Peetermans, *Phys. Rev. Lett.* **1985**, *55*, 2455.

[43] M. Shibayama, K. Nagai, *Macromolecules* **1999**, *32*, 7461.

[44] M. D. Butler, T. D. Montenegro-Johnson, *J. Fluid Mech.* **2022**, *947*, A11.

[45] Y. N. V. Kodakkadan, C. Maslen, P. Cigler, F. Štěpánek, I. Rehor, *J. Mater. Chem. B* **2021**, *9*, 4718.

[46] M. Doi, *J. Phys. Soc. Jpn.* **2009**, *78*, 052001.

[47] T. Tanaka, L. O. Hocker, G. B. Benedek, *J. Chem. Phys.* **1973**, *59*, 5160.

[48] J. J. Bowen, M. A. Rose, A. Konda, S. A. Morin, *Angew. Chem.* **2018**, *130*, 1250.

[49] C. Coulais, A. Sabbadini, F. Vink, M. van Hecke, *Nature* **2018**, *561*, 512.

[50] H. D. McClintock, N. Doshi, A. Iniguez-Rabago, J. C. Weaver, N. T. Jafferis, K. Jayaram, R. J. Wood, J. T. Overvelde, *Adv. Funct. Mater.* **2021**, *31*, 46.